Materials Research Bulletin 136 (2021) 111153

Contents lists available at ScienceDirect

Materials Research Bulletin

journal homepage: www.elsevier.com/locate/matresbu

Spin Seebeck coefficients of Fe, Co, Ni, and $Ni_{80}Fe_{20}$ 3d-metallic thin films

Dongchao Yang [a], Lizhi Yi [a], Shuaiwei Fan [a], Xiaogang He [a], Yunli Xu [a], Min Liu [a], Linjie Ding [a], Liqing Pan [a,*], John Q. Xiao [b,*]

[a] Hubei Engineering Research Center of Weak Magnetic-field Detection, College of Science, China Three Gorges University, Yichang, 443002, China
[b] Department of Physics and Astronomy, University of Delaware, Newark, DE, 19716, USA

ARTICLE INFO

Keywords:
A. Magnetic materials
A. Metals
A. Thin films
D. Spin Seebeck effect
D. Anomalous Nernst effect

ABSTRACT

It is challenge to quantitatively determine the spin Seebeck effect (SSE) of ferromagnetic metals (FM) due to many other thermoelectric signals including the anomalous Nernst effect (ANE), magnetic proximity-induced ANE, and inverse spin Hall effect (ISHE) in FM. By comparing the thermoelectric signals of single FM layer and FM/Pt bilayer and model-assisted analyses of ISHE contribution in FM, we are able to determine the pure SSE signals and the spin Seebeck coefficients of Fe, Co, Ni, and $Ni_{80}Fe_{20}$ over a temperature range from 90 to 300 K. The spin-dependent Seebeck coefficients $S_\uparrow$ and $S_\downarrow$, which is related to the density of states of FM, were also determined experimentally by combining the conventional Seebeck coefficient and the SSE coefficient. We further suggest the calculation of the SSE coefficient should include the spin-dependent conductivities via $S_s \equiv \frac{\sigma_\uparrow S_\uparrow - \sigma_\downarrow S_\downarrow}{\sigma_\uparrow + \sigma_\downarrow}$.

1. Introduction

Spin caloritronics [1] explores the interplay between heat, spin, and charge currents in magnetic structures. Similar to the electrical field, the heat can also be used to manipulate the spin current. One of the most attractive phenomena in spin caloritronics is the spin Seebeck effect (SSE), which was realized experimentally by Uchida et al. in 2008 [2]. In ferromagnet (FM)/normal metal (NM) heterostructures, a temperature gradient can inject spin current from FM into NM layer in which the spin current is converted into a charge current via inverse spin Hall effect (ISHE). In the past decade, the investigation of SSE focuses on not only enhancing the SSE voltage to meet thermoelectric applications [3], but also exploring the spin-related physics, such as long-range spin transport [4], ultrafast spin dynamics [5], etc. The research on SSE has potential for various applications including spin-based storage and computing devices [6], ultra-high frequency (>GHz) microwave emitters or detectors [7], nano-oscillators [8].

Recently, the longitudinal spin Seebeck effect (LSSE) configuration with an out-of-plane temperature gradient is generally accepted as a simple measurement geometry in which the heat flow can be easily controlled. The figure of merit of LSSE devices depends greatly on the SSE coefficients of the FM/NM bilayer systems [3], which can be adjusted separately to enhance the SSE in NM and FM. For NM layers, a large number of experimental data reveals that the spin Hall angle roughly follows a linear dependence of Z^4, which is the atomic number [9]. Until now, 5d metals and their alloys, such as Ta, W, Pt, and IrMn [10], are commonly used because of their strong spin-orbit coupling. For FM layers, the LSSE has been observed in various materials, such as ferromagnetic metals [11,12], semiconductors [13], insulators [14], and recently antiferromagnetic materials [15,16]. Choosing the proper FM materials is still a key point to generate large spin current or raise SSE thermoelectric efficiency. Here, we focus on the SSE of ferromagnetic metals.

Ferromagnetic metals are important spin caloric materials, and it is challenge to accurately determine SSE coefficients in FMs. The first reason is that the thermoelectric signals of a FM/NM bilayer contain many other contributions, which include the anomalous Nernst effect (ANE) and ISHE in FM, and magnetic proximity effect (MPE) induced ANE in heavy metal detection layer such as Pt or Pd. A few strategies have been proposed to measure pure LSSE signal in FM/NM systems. For example, an antiferromagnetic layer was inserted between FM and NM layers to isolate the charge current and transmit the spin current from FM to NM [17]. But it is difficult to measure the attenuation of spin current across the antiferromagnetic layer. The other method used zero ANE material [18], but this method is only suitable for specific FMs. The second reason is that it is difficult to determine the actual temperature

* Corresponding authors.
E-mail addresses: lpan@ctgu.edu.cn (L. Pan), jqx@udel.edu (J.Q. Xiao).

https://doi.org/10.1016/j.materresbull.2020.111153
Received 14 July 2020; Received in revised form 4 November 2020; Accepted 24 November 2020
Available online 1 December 2020

difference on films in LSSE configuration, which causes a large error in determining the LSSE coefficient, even in ferromagnetic insulator system [19]. To accurately determine the temperature gradient, Sola et al. [20] proposed that the heat flux method is more reliable than directly measure the temperature difference on samples because of the uncertainty in thermal contact resistance between samples and heat bath.

In Section 3.1, we analyzed all interfering signals to separate LSSE. In FM/Pt bilayers, we subtracted the ANE and ISHE signals measured in FM single layer and the MPE-induced ANE in Pt layer. With the heat-driven spin transport model, we found that the contribution of the ISHE from FM is comparable to that from Pt. We simulated this process and subtracted it from the SSE signals. Thus, we quantitatively separated LSSE current in FM/Pt. In Section 3.2, after careful calibrating the temperature gradient on films, we are able to determine the temperature-dependent SSE of Fe, Co, Ni, and $Ni_{80}Fe_{20}$ (Py). In Section 3.3, we further determined the spin-dependent Seebeck coefficients $S_\uparrow$ and $S_\downarrow$, which roughly match with their electronic structures, thereby validating our experimental procedures. In Section 3.4, the SSE coefficients of Fe, Co, Ni, and Py are given via $S_s \equiv \frac{\sigma_\uparrow S_\uparrow - \sigma_\downarrow S_\downarrow}{\sigma_\uparrow + \sigma_\downarrow}$.

2. Material and methods

All samples of FM(30)/Pt(4) bilayers, where FM are Fe, Co, Ni, and Py and the number inside the parenthesis is the thickness in unit of nm, were deposited by dc magnetron sputtering on Si(0.5 mm)/ SiO_2(500 nm) substrates with lateral dimensions of 3 mm × 7 mm. The base pressure of the sputtering system is better than 2×10^{-4} Pa. Single FM layer of 30 nm thick were also deposited to subtract the ANE and the ISHE induced by FM from the mixing signals in FM/Pt bilayers. On all samples, two 5-nm Au electrodes were deposited on both ends of the film to eliminate contact resistance. Finally, an AlO_X capping layer was made by depositing 1 nm Al film which was subsequently exposed to air. Film thickness was measured by atomic force microscopy (Innova, Bruker Co.). The magnetic properties were investigated in a vibrating sample magnetometer (Versalab, Quantum Design Co.).

The SSE experiments were performed in a self-modified LSSE configuration as shown in Fig. 1(a). A chip resistor of 1 kΩ was used as a heater, which can provide up to 1 W heating power. A 0.5 mm thick aluminum nitride (AlN) ceramic piece was inserted between the heater and sample for electrical insulation. The sample was placed on a thick Cu block with thermal grease. Constant pressure was applied to ensure good thermal contacts at interfaces. The temperature difference of a few Kelvin across the sample is measured by two Cernox thermometers. The entire setup was placed in and in vacuum to avoid thermal convection. The two-electrode method was used for testing, in which 25- μm Au wires are bonded to both ends of the film with conductive silver paste. The distance between two probes is 6 mm. As shown in Fig. 1(a, b), by applying a temperature gradient in the z-direction and sweeping the magnetic field in the x-direction, the thermoelectrical voltage was measured in the y-direction with a nano-voltmeter (model 2182, Keithley Co.) with a measurement accuracy of better than 100 nV. The resistance of all samples was measured in the same configuration with Keithley 2000 Multimeter.

3. Results and discussion

3.1. Separation of LSSE signals in FM/Pt bilayer

As shown in Fig. 1(b), the charge current J_c induced in the system can be described by

$$J_c = \theta_{SH}\hat{\sigma} \times J_s \quad (1)$$

where J_S is the injected spin current from FM to NM, $\hat{\sigma}$ is the spin-polarization vector determined by the magnetization direction which is in the direction of the applied magnetic field, and θ_{SH} is the spin Hall angle of NM. In FM, the ANE voltage is also be generated in the same direction as the SSE signal [21], which can be described by

$$E_{ANE} = -\alpha_N m \times \nabla T \quad (2)$$

where E_{ANE} is the electric field produced by the ANE, α_N is the ANE coefficient, m is the unit vector of the magnetization.

In FM/Pt system, the total thermoelectric current consists of four

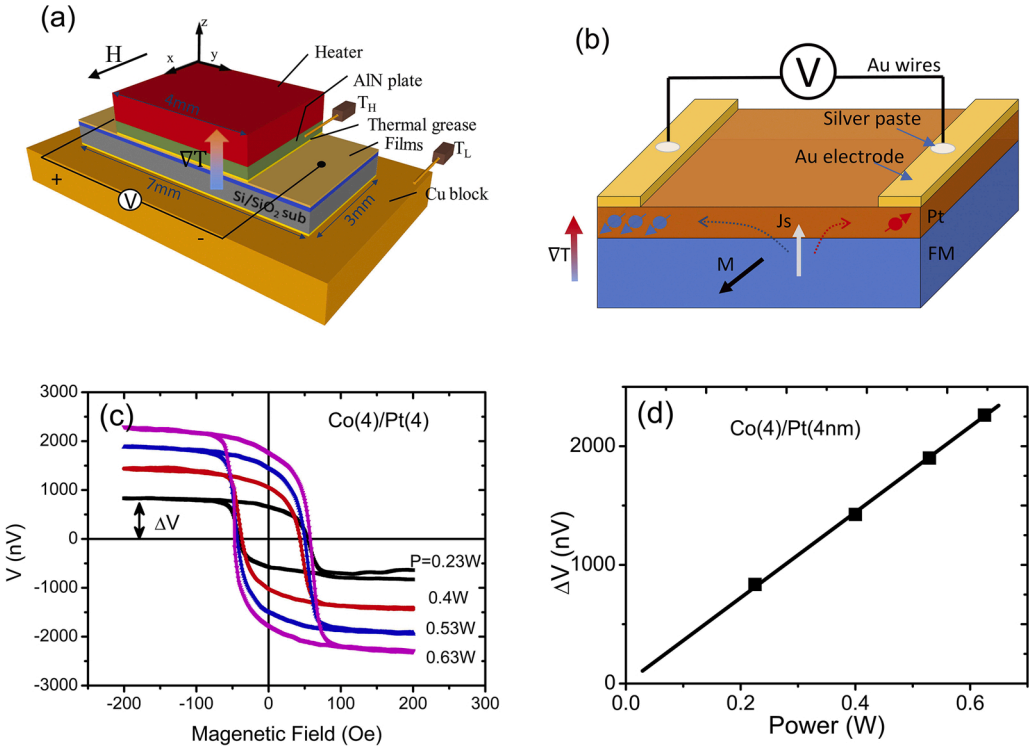

Fig. 1. (a) Experimental setup of LSSE configuration for detecting SSE voltage. T_H (T_L) represents the thermometer at the hot (cold) end. (b) In FM/Pt bilayer, the SSE and ANE signals emerge in the same direction. The arrow in the FM layer denotes the magnetization vector M, the spin current J_s induced by temperature gradient ∇T injected from FM into Pt. (c) The as-measured thermoelectric voltage of a sample by scanning magnetic field and (d) a linear dependence of ΔV on the heating power.

independent current sources in parallel, including intrinsic ANE in FM, MPE-induced ANE of Pt, ISHE induced in FM, and ISHE in Pt, which can be written as

$$I_{FM/Pt} = I_{ANE}^{FM} + I_{ISHE}^{FM} + I_{MPE} + I_{ISHE}^{Pt} \quad (3)$$

To obtain the pure LSSE current I_{ISHE}^{Pt}, we processed the data in the following steps: (1) according to our estimation (see Supplementary), the MPE current was on the order of 1 nA as listed in Table 1. I_{MPE} was treated as a small interfering signal and was subtracted from the total current of FM/Pt bilayer $I_{FM/Pt}$; (2) we measured the ANE (I_{ANE}^{FM}) plus ISHE (I_{ISHE}^{FM}) signals from a single FM layer, which was subtracted from $I_{FM/Pt}$, then we obtained $\Delta I = I_{FM/Pt} - I_{FM} - I_{MPE}$; (3) there is an additional spin current in FM region in FM/Pt bilayer compared with that in single FM layer. This additional spin current introduces ISHE that is not accounted for in ΔI. We estimated this additional ISHE contribution using heat-driven spin transport model and subtracted it from ΔI to get pure I_{ISHE}^{Pt}. We address each step in detail next.

The thermoelectric signal of FM single layers and FM/Pt bilayers were both measured as a function of the magnetic field at 300 K and at a fixed heating power of 0.4 W (Fig. 2(a)). The temperature-dependent thermoelectric current was also plotted in Fig. 2(b) from 90 to 300 K. By taking the current difference $\Delta I = I_{FM/Pt} - I_{FM} - I_{MPE}$, the ANE signal of FM is removed along with part of ISHE contribution. The latter is not completely removed since the spin current distributions are different in FM/Pt bilayers and FM single layers. Based on the thermal-driven spin transport model [18], the spin current distributions in FM/Pt and FM systems are calculated and shown in Fig. 2(c). It is clear that the difference mostly occurs at the FM/NM interface. This difference in spin current (Δj_s) introduces an additional ISHE signal that is not removed by using $\Delta I = I_{FM/Pt} - I_{FM} - I_{MPE}$. We can, however, estimate this additional ISHE contribution.

The ISHE current in a film is $I_{ISHE} = \theta_{SH}\langle J_s\rangle * A_{film}$, where $\langle J_s\rangle = \int_0^t J_s dz * \frac{1}{t}$ is the average spin current in a film, t is the film thickness, the integral area of each curve $\int_0^t J_s dz$ has been shown in Fig. 2(c) labels, A_{film} is the cross-sectional area of ISHE current. The spin Hall angle of a FM (θ_{SH}^{FM}) is comparable to that of Pt with $\theta_{SH}^{FM} = 0.1\sim0.5\,\theta_{SH}^{Pt}$ [22]. Using $\frac{\theta_{SH}^{FM}}{\theta_{SH}^{Pt}} = 0.3$ and the calculated spin current distribution in Fig. 2(c), we obtained the ratio of the additional spin current Δj_s -induced ISHE in FM and the ISHE in Pt is $\frac{\Delta I_{ISHE}^{FM}}{I_{ISHE}^{Pt}} = \frac{0.3\times(24.4-20.1)}{1.34} = 0.96$. The contribution of Δj_s -induced ISHE in the FM region is comparable to that in Pt. Then, we subtract the calculated Δj_s -induced ISHE from $\Delta I = I_{FM/Pt} - I_{FM} - I_{MPE}$ to determine the pure LSSE current in FM/Pt system.

3.2. ΔT calibration method and normalized LSSE voltage $-\frac{\nabla V_{ISHE}}{\nabla T_F}$ in FM/Pt bilayers

With the pure LSSE signal, we still need to accurately determine the temperature difference across the film ΔT_F to determine the LSSE coefficient. Generally, there are two methods to estimate ΔT_F [20]: the temperature difference method and the heat flux method. In the former, the measured temperature difference on sample ΔT consists of three parts: the temperature difference on the film, substrate, and thermal contacts, i.e. $\Delta T = \Delta T_F + \Delta T_{sub} + \Delta T_{contact}$. But the uncertainty in thermal contact resistance at the interfaces between the sample and heat bath cannot be avoided in the longitudinal configuration. So this method is not used here. With the heat flux method, we need to determine the heat flux through the film and the thermal resistance of the film in order to determine $\Delta T_F = P{\cdot}R_h = P{\cdot}\frac{t_F}{\kappa_F{\cdot}A}$, where P, R_h and A are the heater power, the thermal resistance and the surface area of films, respectively. The thermal conductivity κ of films was calculated using the Wiedemann-Franz law $\kappa = \frac{L{\cdot}T}{\rho}$, where L, ρ are the Lorenz constant and electrical resistivity, respectively. Because of the uncertainty in the actual heating power and the Lorenz constant of films, the calculated value could still deviate from the actual ΔT_F. A correction factor F has to be introduced. It should be noted that the ANE coefficient $\alpha_N = -\nabla V_{ANE}/\nabla T_F$ can be measured accurately in the transverse configuration, because there is no uncertain thermal contact resistance (see Supplementary). For convenience, the measured voltage of single-layer FM was regarded as ANE voltage. Using α_N measured in the transverse configuration as shown in Fig. 3(a, b) as the standard values, we corrected the α_N measured in the longitudinal configuration to obtain the correction factor F. It should be pointed out that factor F is a temperature-dependent variable, because as decreasing temperature, the actual heating power on the films would change due to the changing heat dissipation at the other end. Taking the data at 300 K as an example, using $P = 0.4W$, $\kappa_F = 5\mathrm{W/(m{*}K)}$, $t_F = 30nm$, $A = 3\times6mm^2$, $F = 1.6$, the temperature difference and the temperature gradient on the FM were estimated to be 0.09 mK and 2.77 K/mm, respectively. The as-measured resistivity ρ, calibrated temperature gradient ∇T_F, and ANE coefficient α_N are summarized in Fig. 3(c). The temperature-dependent α_N of films show a similar trends as the bulk samples, but the values are smaller compared with their bulk counterparts [23], owing to the finite size effect [24]. The calibration process above ensures an accurate determination of the temperature gradient on films in LSSE configuration.

Analogy to the conventional Seebeck coefficient of FM, the normalized SSE voltage $-\frac{\nabla V_{ISHE}}{\nabla T_F} = -\frac{I_{ISHE}^{Pt} R_{Pt}}{d\,\nabla T_F}$, where d is the length between two contacts, is an important parameter of FM/Pt systems, representing the ability of the FM/Pt system to generate spin currents. To obtain I_{ISHE}^{Pt} of Fe, Co, Ni, and Py, we simulated the spin current distribution using the same method as shown in Fig. 2(c) and determined $\frac{\Delta I_{ISHE}^{FM}}{I_{ISHE}^{Pt}}$ using the corresponding parameters of $\frac{\theta_{SH}^{FM}}{\theta_{SH}^{Pt}}$, $\frac{\sigma_{FM}}{\sigma_{Pt}}$, $\frac{\lambda_{FM}}{\lambda_{Pt}}$, which are also listed in Table 1. At 300 K, taking Py as an example, using $\frac{\theta_{SH}^{Py}}{\theta_{SH}^{Pt}} = 0.2$, $\frac{\sigma_{Py}}{\sigma_{Pt}} = 0.29$, $\frac{\lambda_{Py}}{\lambda_{Pt}} = 3/2$, we determined $\frac{\Delta I_{ISHE}^{FM}}{I_{ISHE}^{Pt}} = 0.39$ (see Supplementary). Then we separated $I_{ISHE}^{Pt} = -3.5\,nA$ from $\Delta I = I_{FM/Pt} - I_{FM} - I_{MPE} = \Delta I_{ISHE}^{FM} + I_{ISHE}^{Pt}$. Using $d = 6$ mm, $R_{Pt} = 130\,\Omega$, $\nabla T_{Py} = 1.7$ K/mm, we obtained $-\frac{\nabla V_{ISHE}}{\nabla T_F} = 0.04\,\mu V/K$. This is consistent with theoretical predicted value of $0.06 \pm 0.04\,\mu V/K$ for Py(30)/Pt(6 nm) [17]. As for the temperature-dependent parameters, we assume constant $\frac{\theta_{SH}^{FM}}{\theta_{SH}^{Pt}}$ and $\frac{\lambda_{FM}}{\lambda_{Pt}}$ because the value of θ_{SH} and λ of FM

Table 1
Parameters used to separate LSSE signal at 300 K. Using the spin Hall angle ($\theta_{SH}^{FM}/\,\theta_{SH}^{Pt}$), spin diffusion length ($\lambda_{FM}/\,\lambda_{Pt}$) from literatures and measured electrical conductivity ($\sigma_{FM}/\,\sigma_{Pt}$), we simulated spin current distribution in FM/Pt bilayers and obtained the ratio $\Delta I_{ISHE}^{FM}/I_{ISHE}^{Pt}$ in the current difference ΔI, which allows us to determine I_{ISHE}^{Pt}. The normalized SSE voltage in FM/Pt system is $-\frac{\nabla V_{ISHE}}{\nabla T_F} = -\frac{I_{ISHE}^{Pt} R_{Pt}}{d\,\nabla T_F}$.

FM	$\frac{\theta_{SH}^{FM}}{\theta_{SH}^{Pt}}$	$\frac{\sigma_{FM}}{\sigma_{Pt}}$	$\frac{\lambda_{FM}}{\lambda_{Pt}}$	$\frac{\Delta I_{ISHE}^{FM}}{I_{ISHE}^{Pt}}$	I_{MPE}(nA)	ΔI(nA)	I_{ISHE}^{Pt}(nA)	∇T_F (K/mm)	$-\frac{\nabla V_{ISHE}}{\nabla T_F}$ ($\mu V/K$)
Fe	0.1 [22]	0.18	2/2 [29]	0.13	−1	−18.7	−16.5	2.77	0.13
Co	0.15 [28]	0.45	40/2 [29]	1.44	−0.8	−23.5	−9.6	1.07	0.20
Ni	0.5 [22]	0.28	3.2/2 [22]	1.04	−0.3	26.2	12.8	1.78	−0.16
Py	0.2 [22]	0.29	3/2 [29]	0.39	−0.5	−4.9	−3.5	1.70	0.04

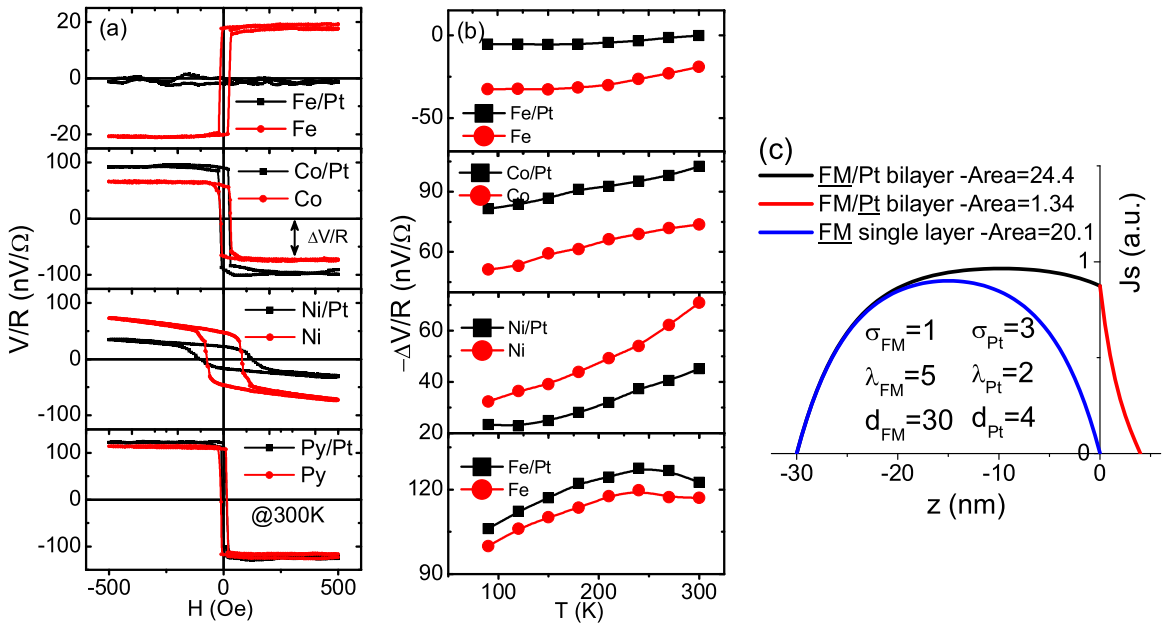

Fig. 2. (a) Thermoelectric current of FM and FM/Pt as a function of the magnetic field at 300 K. (b) Temperature dependence of the thermal-induced current of FM/Pt and FM for Fe, Co, Ni, and Py. (c) Simulation of spin current distribution in the FM and FM/Pt systems according to the model in Ref. [18].

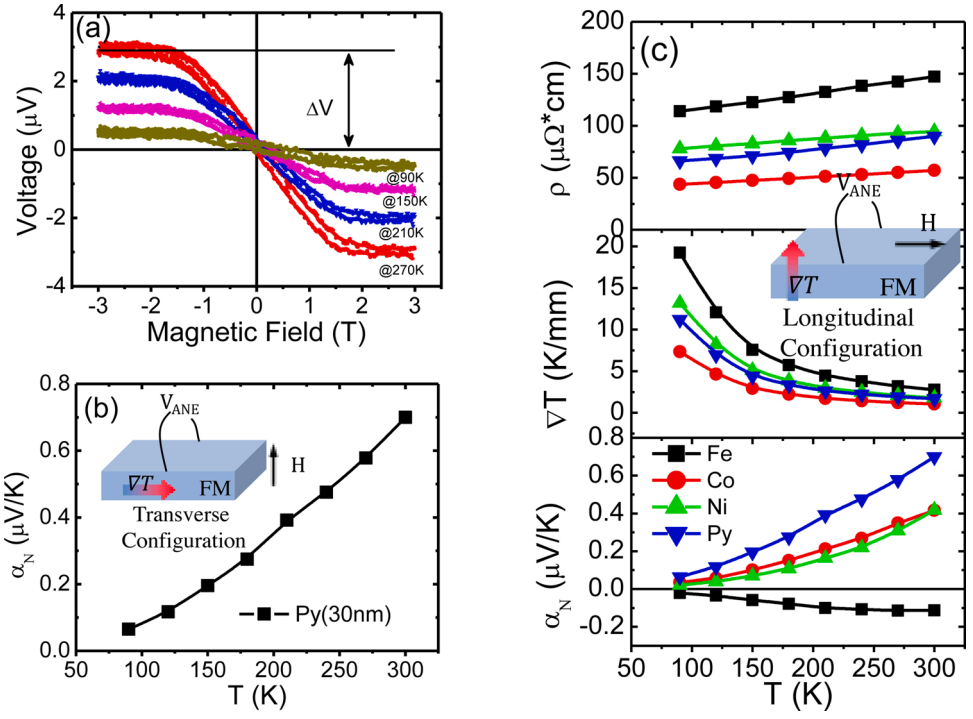

Fig. 3. Method to calibrate the temperature gradient on films in LSSE. In the transverse configuration, (a) the as-measured ANE voltage by scanning magnetic field at different temperature, and (b) the ANE coefficient α_N of Py. (c) In the longitudinal configuration, the as-measured resistivity, the temperature gradient on films and the ANE coefficient of Fe, Co, Ni, and Py after calibration.

and Pt both slightly increase with decreasing temperature [25,26]. Thus, the temperature-dependent $-\frac{\nabla V_{ISHE}}{\nabla T_F}$ was obtained and shown in Fig. 4(a). The absolute value of $-\frac{\nabla V_{ISHE}}{\nabla T_F}$ is ranging from 0 to 0.2 μV/K, which is smaller than the reported value of 0.93 μV/K for YIG/Pt [19]. The value of $-\frac{\nabla V_{ISHE}}{\nabla T_F}$ for Ni has an opposite sign compared to that of Fe, Co and Py, similar to the results reported in earlier studies [27]. This sign difference is attributed to the different electronic structures, which will be discussed next.

3.3. Spin-dependent Seebeck coefficient $S_\uparrow$ and $S_\downarrow$

The spin-dependent Seebeck coefficient $S_\uparrow$ and $S_\downarrow$ can be calculated based on the electronic structure of FM using by the Mott formula [30]

$$S_{\uparrow,\downarrow} = -\frac{\pi^2 k_B^2 T}{3e} \frac{\partial \ln(\sigma_{\uparrow,\downarrow})}{\partial \varepsilon}\Big|_{\varepsilon_F} \quad (4)$$

where k_B is the Boltzmann constant, e is the electric charge, ε_F is the

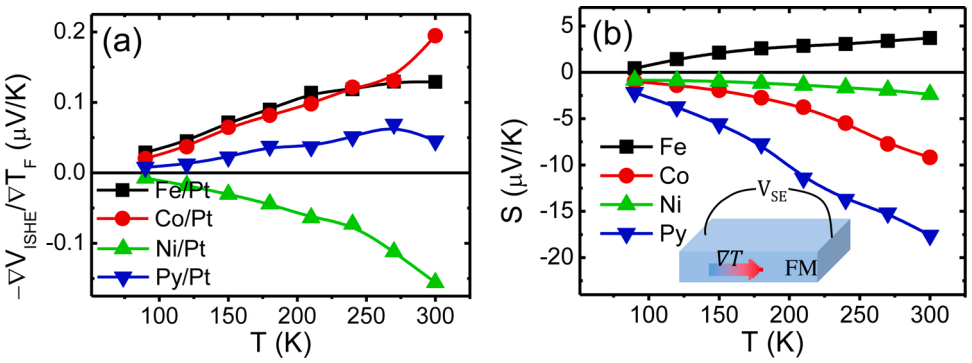

Fig. 4. The temperature dependence of (a) normalized SSE voltage $-\frac{\nabla V_{ISHE}}{\nabla T_F}$ in FM/Pt extracted from the original result shown in Fig. 2 after the temperature gradient calibration, and (b) Seebeck coefficients of FM measured in transverse configuration. The insert shows the measurement geometry.

Fermi energy, T is the temperature, and σ is the conductivity. It is well known that the 4 s electrons are the main carriers in ferromagnetic transition metals, i.e. $\sigma = \sigma_s + \sigma_d \approx \sigma_s$. The conductivity obeys Drude's formula $\sigma_s = \frac{n_s e^2 \tau_s}{m_s^*}$, where the electron density n_s, the effective mass m_s^* are almost the same between the spin-up and spin-down channels due to negligibly small spin splitting of 4 s electrons. But the relaxation time $\tau_{s,\uparrow}$ and $\tau_{s,\downarrow}$ are different depending on the s-d electron scattering, which is asymmetric between two channels due to large spin splitting of 3d electrons. According to the Fermi liquid model [31], the electron scattering cross section for spin-up channel is $\gamma_\uparrow = \gamma_{\uparrow\uparrow} + \gamma_{\uparrow\downarrow}$, including up-up and up-down electron scattering, which can be expressed as:

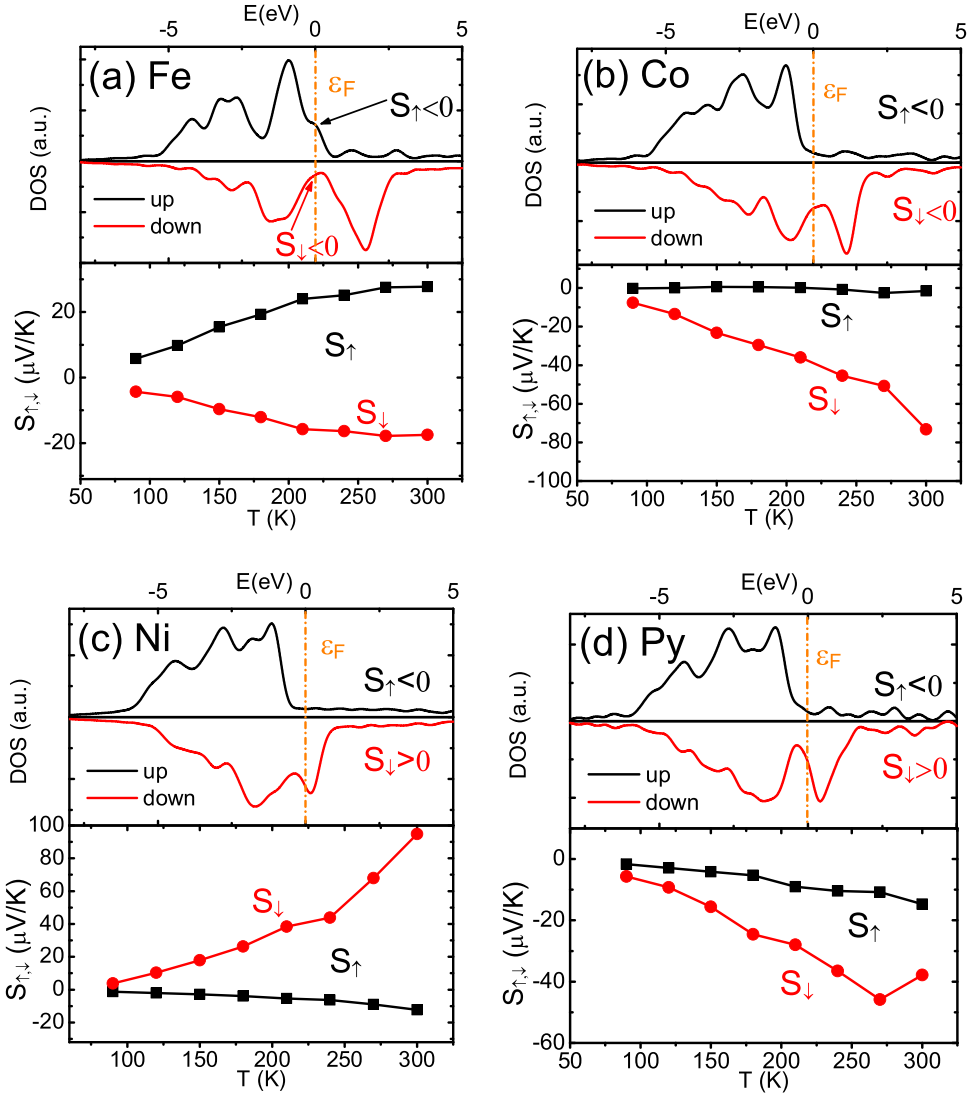

Fig. 5. The calculated spin-up and spin-down DOSs (top panels) and temperature-dependent $S_\uparrow$ and $S_\downarrow$ got from the experiment for (a) Fe, (b) Co, (c) Ni, and (d) Py (bottom panels). The vertical dot line represents the Fermi level ε_F.

$$\gamma_{\uparrow\uparrow} = N_{d,\uparrow}\left(\frac{k_B T}{\varepsilon_{F,\uparrow}}\right)^2 \gamma^0_{\uparrow\uparrow}, \gamma_{\uparrow\downarrow} = N_{d,\downarrow}\left(\frac{k_B T}{\varepsilon_{F,\downarrow}}\right)^2 \gamma^0_{\uparrow\downarrow} \quad (5)$$

where $\gamma^0_{\uparrow\uparrow}$ and $\gamma^0_{\uparrow\downarrow}$ are the cross-sections for a free-electron-gas system, $N_{d,\uparrow}$ and $N_{d,\downarrow}$ are the densities of the states (DOSs) at the Fermi level, $\varepsilon_{F,\uparrow}$ and $\varepsilon_{F,\downarrow}$ are the Fermi energy for the 3d spin-up and spin-down electrons, respectively. Because $\gamma^0_{\uparrow\downarrow} \approx \gamma^0 \ll \gamma^0_{\uparrow\uparrow}$ due to the strong Fermi repulsion, it leads to $\gamma_{\uparrow} \approx \gamma_{\uparrow\uparrow}$. The same result can be obtained for the spin-down channel, i.e. $\gamma_{\downarrow} \approx \gamma_{\downarrow\downarrow}$. Therefore, the spin-dependent relaxation time can be expressed as $\tau_{\uparrow,\downarrow} \propto 1/\gamma_{\uparrow,\downarrow} \propto \varepsilon^2_{F,(\uparrow,\downarrow)}/N_{d,(\uparrow,\downarrow)}$, which leads to $\sigma_{\uparrow,\downarrow} \propto \varepsilon^2_{F,(\uparrow,\downarrow)}/N_{d,(\uparrow,\downarrow)}$. Combining this with the formula (4), $S_{\uparrow,\downarrow}$ approximately depends on the differential of the spin-dependent DOSs at ε_F, i.e. $S_{\uparrow,\downarrow} \propto \partial ln N_{d,(\uparrow,\downarrow)}(\varepsilon)/\partial\varepsilon\big|_{\varepsilon_F}$. The DOSs versus energy for Fe, Co, Ni, and Py are plotted in Fig. 5, and $S_{\uparrow}$ and $S_{\downarrow}$ can be qualitatively acquired.

On the other hand, the spin-dependent Seebeck coefficient $S_{\uparrow}$ and $S_{\downarrow}$ can be obtained from the experiment by combining the values of Seebeck coefficient S and the variable β from LSSE (see Supplementary):

$$S = \frac{\sigma_{\uparrow} S_{\uparrow} + \sigma_{\downarrow} S_{\downarrow}}{\sigma_{\uparrow} + \sigma_{\downarrow}} \quad (6)$$

$$\beta = \frac{1}{\theta_{SH}} \frac{\sigma_N}{\sigma_F} \frac{d_N}{\lambda_N} \frac{1}{tanh\left(\frac{d_N}{2\lambda_N}\right)} \left(-\frac{\nabla V_{ISHE}}{\nabla T_F}\right) = \frac{2\sigma_{\uparrow}\sigma_{\downarrow}}{{\sigma_F}^2}(S_{\uparrow} - S_{\downarrow}) \quad (7)$$

where θ_{SH}, σ, d, λ are spin Hall angle, conductivity, film thickness, and spin diffusion length, respectively. The variable β is determined from the LSSE experiment. Take the data at 300 K as an example, $d_{Pt} = 4\ nm$, $\theta_{SH} = 0.08$, $\lambda_{Pt} = 2\ nm$ [26], $\tanh(1) = 0.76$, $\frac{\sigma_N}{\sigma_F} = 2 \sim 5$ for different FM, the results of β at 300 K are listed in Table 2. As for temperature-dependent parameters, the spin Hall angle of Pt remains unchanged at 90−300 K according to the literature. The spin diffusion length is proportional to the conductivity of Pt, which will slightly increase as the temperature decreases from 300 to 90 K [26]. To get $S_{\uparrow}$ and $S_{\downarrow}$ of FM, we should also determine the asymmetry coefficient of spin-dependent conductivity $g = \sigma_{\uparrow}/\sigma_{\downarrow}$ according to $\sigma_{\uparrow,\downarrow} \propto \varepsilon^2_{F,(\uparrow,\downarrow)}/N_{d,(\uparrow,\downarrow)}$, where $\varepsilon_F = \frac{\hbar^2}{2m}\left(\frac{3\pi^2 n}{V}\right)^{2/3}$ can be used, $N_{d,(\uparrow,\downarrow)}$ is determined from the calculated DOSs. The obtained values of $g = \sigma_{\uparrow}/\sigma_{\downarrow}$ is shown in Table 2. Due to $\sigma \propto \tau \propto \lambda$, we compared the calculated $\sigma_{\uparrow}/\sigma_{\downarrow}$ and the spin-dependent mean free path ratio $\lambda_{\uparrow}/\lambda_{\downarrow}$ in literature [32], we note that $g \gg 1$ for Co, Ni, Py in agreement with that of $\lambda_{\uparrow} \gg \lambda_{\downarrow}$, and $g < 1$ for Fe since its $\lambda_{\uparrow} < \lambda_{\downarrow}$ as well. The spin-dependent Seebeck coefficient $S_{\uparrow} = S + \frac{g+1}{2g}\beta$ and $S_{\downarrow} = S - \frac{g+1}{2}\beta$ of Fe, Co, Ni, and Py can be obtained and the results are shown in Fig. 5.

Fig. 5 shows the DOSs obtained by ab initio calculation and the experimental values of the spin-dependent Seebeck coefficient $S_{\uparrow}$ and $S_{\downarrow}$ for FM. For Ni, the experimental results are consistent with the values estimated from the DOSs by $S_{\uparrow,\downarrow} \propto \partial ln N_{d,(\uparrow,\downarrow)}(\varepsilon)/\partial\varepsilon\big|_{\varepsilon_F}$ that $S_{\uparrow}$ is close to zero while $S_{\downarrow}$ has a large positive value, leading to a negative spin Seebeck coefficient S_s (see next section). For other three metals, the values of $S_{\uparrow}$ and $S_{\downarrow}$ deviate a little bit from the values calculated from DOSs. This is mainly due to the value of $g = \frac{\sigma_{\uparrow}}{\sigma_{\downarrow}}$, which has a great influence on the determination of $S_{\uparrow}$ and $S_{\downarrow}$, is calculated based on a simplified model. The actual conductivity is more complicated because of the hybrid 4 s and 3d energy bands [33]. The obtained $S_{\uparrow}$ and $S_{\downarrow}$ from the experiment roughly linearly depend on temperature, indicating that the conduction electrons are the main carriers of the spin current in the ferromagnetic metals. More importantly, similar to the conventional Seebeck effect [34] where doped impurity in PbTe can enhance the Seebeck coefficient by distorting DOSs, the spin Seebeck coefficient may also be enhanced by tailoring the energy band structure of FM.

3.4. Definition and Results of Spin Seebeck Coefficient S_s

Spin Seebeck effect is derived based on the conventional Seebeck effect with spin up and spin down electrons. The definition of $S_s \equiv (S_{\uparrow} - S_{\downarrow})$ is commonly used [35], but it ignores the effect of the spin-dependent conductivity. The correct expression should be [36]

$$S_s \equiv \frac{\sigma_{\uparrow} S_{\uparrow} - \sigma_{\downarrow} S_{\downarrow}}{\sigma_{\uparrow} + \sigma_{\downarrow}} \quad (8)$$

The calculated spin Seebeck coefficients for Fe, Co, Ni, and Py are shown in Fig. 6. The calculated S_s of Ni has opposite sign to those of Fe and Co. But for Py, although the SSE transport coefficient of Py is positive, S_s change the sign by taking into account the spin-dependent conductivities.

4. Conclusions

In summary, we have carefully analyzed all possible thermoelectric signals in single FM layers and FM/Pt bilayers. The MPE current was estimated and subtracted from the total current of FM/Pt bilayers. While ANE and part of ISHE signals in FM layer can be removed by taking the difference between signals in FM/Pt and FM systems, the additional spin current in FM/Pt compared with that in single FM layer cannot be

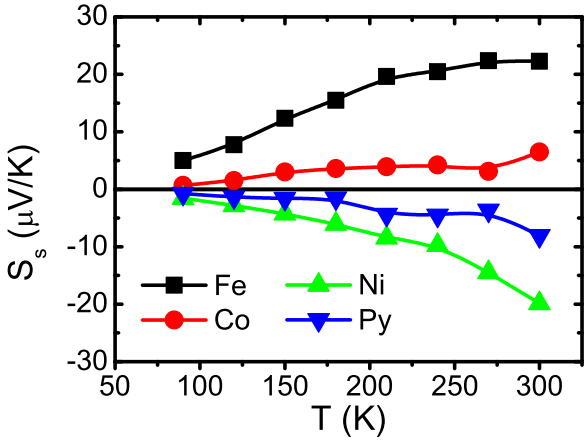

Fig. 6. The temperature-dependent spin Seebeck coefficients for Fe, Co, Ni, Py determined from Eq. (8).

Table 2
Parameters used in calculating the spin-dependent Seebeck coefficient $S_{\uparrow}$ and $S_{\downarrow}$ at 300 K. M_s is the saturation magnetic moment, $n_{\uparrow}$ ($n_{\downarrow}$) is the total number of 3d electrons, ε_F is the Fermi energy, $N_{d,\uparrow}$ ($N_{d,\downarrow}$) is the 3d electron DOSs at ε_F, $\sigma_{\uparrow}$ ($\sigma_{\downarrow}$) is the spin-dependent conductivity, $\lambda_{\uparrow}$ ($\lambda_{\downarrow}$) is the electron mean free path from Ref. [32]. β and S are obtained from the experiment at 300 K. Thus, we obtained $S_{\uparrow} = S + \frac{g+1}{2g}\beta$ and $S_{\downarrow} = S - \frac{g+1}{2}\beta$.

FM	M_s (μ_B)	$n_{\uparrow}$	$n_{\downarrow}$	$\frac{\varepsilon^2_{F,\uparrow}}{\varepsilon^2_{F,\downarrow}}$	$\frac{N_{d,\downarrow}}{N_{d,\uparrow}}$	$\frac{\sigma_{\uparrow}}{\sigma_{\downarrow}}$	$\frac{\lambda_{\uparrow}}{\lambda_{\downarrow}}$	β ($\mu V/K$)	S ($\mu V/K$)	$S_{\uparrow}$ ($\mu V/K$)	$S_{\downarrow}$ ($\mu V/K$)
Fe	2.2	4	2.6	2.26	0.39	0.88	1.5/2.1	22.5	3.7	28	−17
Co	1.7	8	3.3	1.74	4.8	8.35	5.5/0.6	13.7	−9.2	−2	−73
Ni	0.6	5	4.4	1.19	8.3	9.84	\	−17.9	−2.4	−12	95
Py	1	5	4	1.39	5	6.95	4.6/0.6	5.1	−17.6	−15	−38

removed. Through modeling, we have found that this addition ISHE contribution in FM part of FM/Pt bilayers is comparable to that generated in Pt layer. By removing this contribution using calculated values, we are able to determine the pure LSSE signal in FM/Pt systems. With the definition of SSE coefficient $S_s \equiv \frac{\sigma_\uparrow S_\uparrow - \sigma_\downarrow S_\downarrow}{\sigma_\uparrow + \sigma_\downarrow}$, we have found that Ni and Py have negative S_s that is opposite to Fe and Co. In addition, we have also determined the spin-dependent Seebeck coefficient $S_\uparrow$ and $S_\downarrow$, which is roughly in agreement with the calculated values from DOSs at the Fermi level. Our results show the direct correlation between the electronic structure and thermal-driven spin transport in 3d-FM metals are explored, which may also help improve thermal-driven spin currents efficiency in 3d-FM metals in the future study.

Declaration of Competing Interest

The authors declare that they have no known competing financial interests or personal relationships that could have appeared to influence the work reported in this paper.

Acknowledgements

The author D. Yang thanks Mr. Zhu Wang for the help in ab initio calculation. This work was supported by National Natural Science Foundation of China (Grant No.: 51371105), Prof. J. Q. Xiao was supported by National Science Foundation of USA (Grant No.: DMR1505592).

Appendix A. Supplementary data

Supplementary material related to this article can be found, in the online version, at doi:https://doi.org/10.1016/j.materresbull.2020.111153.

References

[1] G.E.W. Bauer, E. Saitoh, B.J. Van Wees, Nat. Mater. 11 (2012) 391.
[2] K. Uchida, S. Takahashi, K. Harii, J. Ieda, W. Koshibae, K. Ando, S. Maekawa, E. Saitoh, Nature 455 (2008) 778.
[3] K. Uchida, H. Adachi, T. Kikkawa, A. Kirihara, M. Ishida, S. Yorozu, S. Maekawa, E. Saitoh, P. IEEE 104 (2016) 1946.
[4] B. Giles, Z. Yang, J. Jamison, R. Myers, Phys. Rev. B 92 (2015), 224415.
[5] J. Kimling, G. Choi, J.T. Brangham, T. Matalla-Wagner, T. Huebner, T. Kuschel, F. Yang, D.G. Cahill, Phys. Rev. Lett. 118 (2017) 57201.
[6] G. Csaba, Á. Papp, W. Porod, Phys. Lett. A 381 (2017) 1471.
[7] N. Locatelli, V. Cros, J. Grollier, Nat. Mater. 13 (2014) 11.
[8] C. Safranski, et al., Nat. Commun. 8 (2017) 117.
[9] H.L. Wang, C.H. Du, Y. Pu, R. Adur, P.C. Hammel, F.Y. Yang, Phys. Rev. Lett. 112 (2014), 197201.
[10] J.B.S. Mendes, R.O. Cunha, O.A. Santos, P.R.T. Ribeiro, F.L.A. Machado, R. L. Rodrínguez-Suárez, A. Azevedo, S.M. Rezende, Phys. Rev. B 89 (2014), 140406.
[11] K. Lee, et al., Sci. Rep. 5 (2015) 10249.
[12] Y. Xu, B. Yang, C. Tang, Z. Jiang, M. Schneider, R. Whig, J. Shi, Appl. Phys. Lett. 105 (2014), 242404.
[13] C.M. Jaworski, J. Yang, S. Mack, D.D. Awschalom, J.P. Heremans, R.C. Myers, Nat. Mater. 9 (2010) 898.
[14] K. Uchida, et al., Nat. Mater. 9 (2010) 894.
[15] S. Seki, T. Ideue, M. Kubota, Y. Kozuka, R. Takagi, M. Nakamura, Y. Kaneko, M. Kawasaki, Y. Tokura, Phys. Rev. Lett. 115 (2015), 266601.
[16] P.R.T. Ribeiro, F.L.A. Machado, M. Gamino, A. Azevedo, S.M. Rezende, Phys. Rev. B 99 (2019) 94432.
[17] J. Holanda, O.A. Santos, R.O. Cunha, J.B.S. Mendes, R.L. Rodríguez-Suárez, A. Azevedo, S.M. Rezende, Phys. Rev. B 95 (2017), 214421.
[18] H. Kannan, X. Fan, H. Celik, X. Han, J.Q. Xiao, Sci. Rep. 7 (2017) 6175.
[19] A. Sola, et al., IEEE T. Instrum. Meas. 68 (2019) 1765–1773.
[20] A. Sola, P. Bougiatioti, M. Kuepferling, D. Meier, G. Reiss, M. Pasquale, T. Kuschel, V. Basso, Sci. Rep. 7 (2017) 46752.
[21] K. Hasegawa, M. Mizuguchi, Y. Sakuraba, T. Kamada, T. Kojima, T. Kubota, S. Mizukami, T. Miyazaki, K. Takanashi, Appl. Phys. Lett. 106 (2015), 252405.
[22] C. Du, H. Wang, F. Yang, P.C. Hammel, Phys. Rev. B 90 (2014), 140407.
[23] S.J. Watzman, R.A. Duine, Y. Tserkovnyak, S.R. Boona, H. Jin, A. Prakash, Y. Zheng, J.P. Heremans, Phys. Rev. B 94 (2016), 144407.
[24] T.C. Chuang, P.L. Su, P.H. Wu, S.Y. Huang, Phys. Rev. B 96 (2017), 174406.
[25] M. Isasa, E. Villamor, L.E. Hueso, M. Gradhand, F. Casanova, Phys. Rev. B 91 (2015), 024402.
[26] Y. Wang, P. Deorani, X. Qiu, J.H. Kwon, H. Yang, Appl. Phys. Lett. 105 (2014), 152412.
[27] K. Uchida, T. Ota, K. Harii, K. Ando, H. Nakayama, J. Appl. Phys. 107 (2010) 9A.
[28] D. Tian, Y. Li, D. Qu, X. Jin, C.L. Chien, Appl. Phys. Lett. 106 (2015), 212407.
[29] J. Bass, W.P. Pratt Jr., J. Phys.-Condens. Mat. 19 (2007), 183201.
[30] K. Behnia, Fundamentals of Thermoelectricity, Oxford University Press, New York, 2020.
[31] C. Kittel, Introduction to Solid State Physics, 8th edn, John Wiley & Sons, New York, 2020, p. 417.
[32] B.A. Gurney, V.S. Speriosu, J.P. Nozieres, H. Lefakis, D.R. Wilhoit, O.U. Need, Phys. Rev. Lett. 71 (1993) 4023.
[33] M.S. Bahramy, P. Murugan, G.P. Das, Y. Kawazoe, Phys. Rev. B 75 (2007), 054404.
[34] J.P. Heremans, V. Jovovic, E.S. Toberer, A. Saramat, K. Kurosaki, A. Charoenphakdee, S. Yamanaka, G.J. Snyder, Science 321 (2008) 554.
[35] A. Slachter, F.L. Bakker, J. Adam, B.J. Van Wees, Nat. Phys. 6 (2010) 879.
[36] L. Yi, D. Yang, M. Liu, H. Fu, L. Ding, Y. Xu, B. Zhang, L. Pan, J.Q. Xiao, Adv. Funct. Mater. 30 (2020), 2004024.